

# Carboxylated Ficolls: Preparation, Characterization, and Electrophoretic Behavior of Model Charged Nanospheres

Xuhong Guo,<sup>\*,†</sup> Gavin F. Kirton, and Paul L. Dubin<sup>\*</sup>

Department of Chemistry, Indiana University-Purdue University, Indianapolis, 402 N. Blackford Street, Indianapolis, Indiana 46202-3274

Received: May 1, 2006; In Final Form: August 20, 2006

Carboxylated ficolls were prepared as model spherical colloids of variable charge and size, with radii ranging from 3.0 to 19.3 nm. Capillary electrophoresis (CE), electrophoretic light scattering (ELS), and potentiometric titration were used to determine mobilities as a function of pH, degree of ionization  $\alpha$ , and surface potential  $\psi_0$ . Measured mobilities typically display a plateau at high pH, corresponding to high  $\alpha$  and  $\psi_0$ , confirming the general nature of this effect for charged spheres, seen also for charged dendrimers and charged latex particles. This result is examined in the context of a discontinuity in mobility predicted by the Wiersema, O'Brien, and White (WOW) theory and a more recent primitive model electrophoresis (PME) theory, in which bound counterions are considered either as point charges or as hard spheres. While no mobility maximum can be determined as expected by these two theories, our data seem more to support Belloni's theoretical expectations on charged polymers and spheres. Here we explain the mobility plateaus in terms of counterions accumulated close to the surface (surface potential-determining ions) or within the shear plane (mobility-determining ions).

## Introduction

A central task in understanding the electrostatic properties of colloidal dispersions and protein solutions is providing a description of the electric double layer (EDL), defined as the electrolyte structure around a charged particle. Electrophoresis is a powerful and convenient way to investigate the EDL because the motion of charged particles in external electric fields reflects its strong influence. Two modern techniques, capillary electrophoresis (CE) and electrophoretic light scattering (ELS), allow for direct measurement of the electrophoretic mobility ( $\mu$ ) of charged particles. The main objective of theoretical studies is to correlate the measured mobility with the charge and shape of the particle and the ionic character of the medium.<sup>1</sup> The mobility is often parametrized in terms of the  $\zeta$  potential, the mean electrostatic potential at the shear plane, but since there is no experimental method to define the shear plane for small colloid particles, the significance of  $\zeta$  is highly model-dependent. In the classical theory of Wiersema,<sup>2</sup> O'Brien, and White<sup>3</sup> (WOW), the mobility arises from a balance among electric force, hydrodynamic drag, and relaxation effects. The charged particle is considered as a hard sphere of uniform surface charge density ( $\sigma$ ) surrounded by point-charge counterions, and the static spherical electrical double layer is treated by the Poisson–Boltzmann theory. One result of WOW theory is a maximum in the dependence of  $\mu$  on the surface charge density when the Debye length,  $\kappa^{-1}$ , is small compared to the particle radius  $a$ , i.e., when  $\kappa a > 3$ . The reason for the maximum in the mobility is that the electrophoretic retarding forces which act on a particle increase more rapidly with  $\zeta$  potential (proportional to  $\zeta^2$ ) than

does the driving force (proportional to  $\zeta$ ).<sup>3</sup> A maximum is also found in the more recent primitive model electrophoresis theory (PME) of Lozada-Cassou et al.,<sup>1,4–6</sup> which considers the surrounding counterions as hard spheres of finite size and employs the so-called hyper-netted-chain/mean-spherical approximation (HNC/MSA) including ion–ion correlations.<sup>6,7</sup> The dependence of mobility on  $\sigma$  and  $\kappa a$  is not considered to be universal, as in WOW, but also depends on counterion radii. In the case of low ionic strength, low  $\sigma$ , and negligible counterion size, PME reduces to WOW.<sup>1</sup>

While extensive theoretical investigations of the relationship between the electrophoretic mobility and the surface charge density of spheres have been reported,<sup>1–7</sup> experimental data to confirm e.g. the maximum in  $\mu$ – $\sigma$  curves are rare. One possible reason may be the absence of model compounds that combine spherical symmetry with systematic control of size and charge density. In the range of a few hundred nanometers, surface charged polystyrene latexes have been employed. Martin-Molina et al. investigated such materials (particle size, 180 and 280 nm, and maximum surface charge density,  $-1.75$  and  $-0.22$  C/m<sup>2</sup>, respectively) and observed a plateau in the  $\mu$ – $\sigma$  curve.<sup>8</sup> The same phenomenon was found by Schulz et al.<sup>9</sup> for 100 and 131 nm sulfated or carboxylated latex particles. For the much smaller particle size range of several nanometers, Hoagland et al.<sup>10</sup> and Dubin et al.<sup>11</sup> studied the mobility of charged dendrimers (for example, in ref 11, carboxyl-terminated “G2” and “G5” dendrimers with hydrodynamic radii: 1.7 and 3.7 nm and maximum surface charge densities  $-0.16$  and  $-0.94$  C/m<sup>2</sup>, respectively) and found plateaus in the  $\mu$ – $\sigma$  curve. This leaves a gap in the particle size range 5–50 nm, in which the relationship among particle charge, size, ionic strength, and mobility is certainly of interest, if only because this includes the size domain of many proteins. However, proteins are very complex with respect to geometry and charge heterogeneity and often aggregate readily. Solutes in this size range more

\* To whom correspondence should be addressed. Tel: (413) 577-4167 (P.L.D.); (609) 258-5185 (X.G.). Fax: (413) 545-4490 (P.L.D.); (609) 258-0211 (X.G.). E-mail: dubin@chem.umass.edu (P.L.D.); xguo@princeton.edu (X.G.).

<sup>†</sup> Present address: Department of Chemical Engineering, Princeton University, Princeton, NJ 08544.

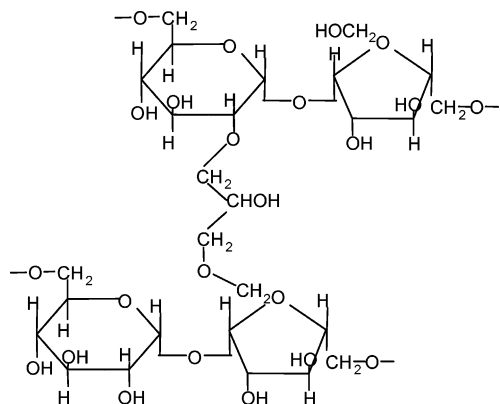


**Figure 1.** Chemical structure of ficoll.

**TABLE 1: Characteristics of Carboxylated Ficoll Fractions**

| sample | $R_h$ (nm) | $10^{-5}M$ (g/mol) | $Q$ (e/molecule)  | $\sigma$ (e/nm <sup>2</sup> ) |
|--------|------------|--------------------|-------------------|-------------------------------|
| CF-1   | 3.0        | 0.2                | $5.9 \times 10^1$ | 0.5                           |
| CF-2   | 3.8        | 0.4                | $1.4 \times 10^2$ | 0.8                           |
| CF-3   | 4.7        | 0.6                | $1.7 \times 10^2$ | 0.6                           |
| CF-4   | 6.0        | 1.1                | $4.4 \times 10^2$ | 1.0                           |
| CF-5   | 7.5        | 1.7                | $7.4 \times 10^2$ | 1.0                           |
| CF-6   | 7.8        | 1.9                | $1.3 \times 10^3$ | 1.8                           |
| CF-7   | 8.8        | 2.5                | $1.4 \times 10^3$ | 1.5                           |
| CF-8   | 9.3        | 2.8                | $1.7 \times 10^3$ | 1.6                           |
| CF-9   | 11.3       | 4.2                | $2.3 \times 10^3$ | 1.4                           |
| CF-10  | 12         | 4.8                | $3.0 \times 10^3$ | 1.7                           |
| CF-11  | 13.2       | 5.9                | $3.9 \times 10^3$ | 1.8                           |
| CF-12  | 14.3       | 7.1                | $5.1 \times 10^3$ | 2.0                           |
| CF-13  | 15.5       | 8.4                | $6.2 \times 10^3$ | 2.0                           |
| CF-14  | 16.4       | 9.5                | $6.5 \times 10^3$ | 1.9                           |
| CF-15  | 16.7       | 9.9                | $6.3 \times 10^3$ | 1.8                           |
| CF-16  | 17.0       | 10                 | $7.4 \times 10^3$ | 2.0                           |
| CF-17  | 18.2       | 12                 | $7.9 \times 10^3$ | 1.9                           |

compatible with tests of theory should be nonhydrophobic, spherically symmetrical, with uniform and variable surface charge density.

Ficolls, prepared by cross-linking polysucrose with epichlorohydrin (Figure 1), are highly branched polysaccharides, whose spherical shape and size is retained regardless of solution ionic strength.<sup>12–14</sup> Conversion of surface hydroxyl groups to carboxyl groups offers the possibility of a series of negatively charged spheres of variable size and charge, which should be model solutes for the study of electrophoretic mobility. In this paper, we report on the preparation of carboxylated ficoll samples with sizes between those of dendrimers and latex particles. Their size and charge are characterized by light scattering and potentiometric titration, and their mobilities are measured by CE and ELS. The purpose of this work is to establish the general features of electrophoretic mobility for charged spheres in this size range.

## Experimental Section

**Materials.** Broad molecular weight distribution (MWD) Ficoll 400 was purchased from Pharmacia Biotech (Sweden). Narrow size-distributed ficoll fractions with hydrodynamic radii 3.0, 4.6, and 7.3 nm respectively were obtained from Dr. Rune Andersson of Pharmacia (see Table 1). The DELSA standard sample EMPSL7 (lot no. 3001) was supplied by Coulter Instrument Co. Bovine Serum Albumin (BSA) (lot 16H9317) was from Sigma. Sodium chloroacetate (98%) and sodium hydroxide (NaOH) (98%) were from Aldrich. Ammonium acetate (98.2%) and sodium chloride (NaCl) (99.7%) as well as standard NaOH and hydrochloric acid (HCl) solutions were from Fisher Scientific (Pittsburgh, PA). Milli-Q water was used in all experiments.

**Methods. Carboxylation.** Commercial Ficoll 400 was carboxylated by e.g. dissolving 10 g of Ficoll 400, 200 g of sodium chloroacetate, and 77.6 g of sodium chloride in 370 mL of Milli-Q water and bringing the solution to 60 °C. The reaction was maintained at 60 °C with stirring for 48 h. The degree of carboxylation was monitored by titration of the reactant sample with standard HCl solution before purification.

The solution after reaction was titrated to pH ca. 7 to remove the excessive NaOH and then purified by dialysis (Spectra/Por 6 dialysis membrane with nominal molecular weight cutoff 10 KDa) against Milli-Q water until the conductivity of the outside water became constant, followed by lyophilization. Five carboxylated Ficoll 400 samples prepared with different weight ratios of sodium chloroacetate to Ficoll 400 are designated as CF400(5:1), CF400(10:1), CF400(20:1), CF400(22:1), and CF400(30:1) with sodium chloroacetate:ficoll weight ratios of 5, 10, 20, 22, and 30, respectively. The narrow size-distributed ficoll fractions from Pharmacia were similarly carboxylated with a sodium chloroacetate:ficoll weight ratio 20:1 to yield CF3.0, CF4.6, and CF7.3.

**Fractionation.** To obtain narrow MWD carboxylated ficoll fractions, CF400 was fractionated by preparative size exclusion chromatography (SEC) with an Automated Econo low-pressure chromatography system consisting of a Sephacryl S-300-HR column (2.5 cm diameter, with a packed bed height of 46 cm), a Bio-Rad EP-1 pump, and a model 2110 fraction collector. The mobile phase (pH = 7.0) 0.1 M ammonium acetate was eluted at 2.0 mL/min. After each fraction was subjected to analytical SEC (see below), the fractions with identical elution volumes were pooled and then lyophilized.

**Analytical Size Exclusion Chromatography (SEC).** Analytical SEC was performed on an apparatus comprised of a NSI-33R Milton Roy minipump (Riviera Beach, FL), a Rheodyne (Cotati, CA) model 7010 injector with a 100  $\mu$ L sample loop, a Gilson (Middleton, WI) 112 UV/vis detector, and a Waters Associates-Millipore (Milton, MA) R401 differential refractometer, coupled to a Kipp and Zonen two-channel recorder. A Superose 6 HR 10/30 column from Pharmacia Biotech (Piscataway, NJ) was connected between the injector and detectors. Flow rates were determined by weighing of timed collections of eluant and were reproducible to within  $\pm 1\%$ . Chart recorder speed was usually 1 cm/min and determined to within  $\pm 1\%$ . All measurements were done at room temperature. Injections were performed in a mobile phase of 0.1 M ammonium acetate buffer, which was filtered with 0.45  $\mu$ m Acetate Plus filters (MSI, MA) and degassed before using. Calibration of the column was accomplished using pullulan standards (TosoHaas, Tokyo).

**Dynamic Light Scattering (DLS).** Dynamic light scattering (DLS) measurements were performed at  $25 \pm 1$  °C at 90° scattering angle using a Brookhaven Instruments system equipped with a 256-channel digital correlator (BI-9000AT) and an Omnicrome air-cooled 200 mW argon-ion laser (532R-MBS-A04) operating at a vacuum wavelength of 488 nm.

**Potentiometric Titration.** To determine the total surface charges of carboxylated ficoll fractions as well as the relationship between pH and the degree of ionization ( $\alpha$ ), potentiometric titrations with 0.1 M HCl or 0.1 M NaOH were performed with an Orion pH meter 811 at  $23 \pm 1$  °C, calibrated with pH 4.00  $\pm 0.01$  and 7.00  $\pm 0.01$  buffers just before titration. The instrumental drift was less than 0.02 pH units during titration. Nitrogen gas N<sub>2</sub> was bubbled through the solution for 5 min to remove carbon dioxide before the titration, and all the titrations were performed under N<sub>2</sub>. A 2.0 mL microburet was used to add standard NaOH or HCl solutions to a 5.00 mL aqueous

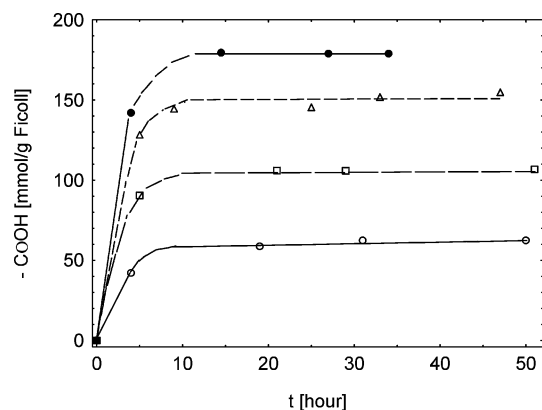


**Figure 2.** Degree of carboxylation as a function of reaction time. Weight ratio (C/F) of sodium chloroacetate to ficoll (from top to bottom): C/F = 20 (●); C/F = 30 (△); C/F = 10 (□); C/F = 5 (○).

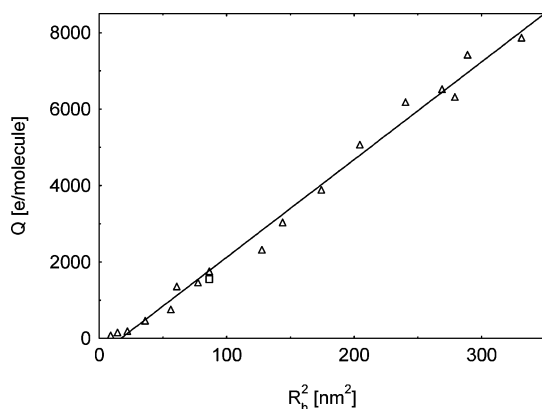


**Figure 3.** Average charge amount  $Q$  as a function of the square of hydrodynamic radii for fractionated carboxylated ficolls (△) and parent sample CF400(20:1) (□).

solution of carboxylated ficoll samples adjusted to the desired ionic strength with NaCl. Blank titrations were always performed before and after the sample titrations.

**Capillary Electrophoresis.** CE was carried out on a Beckman P/ACE 5500 instrument using a 50  $\mu\text{m}$  inner diameter uncoated capillary, 27 cm total length and 19.25 cm effective length (from injection end to detection window), operating at 5–30 kV. The temperature was maintained at  $25.0 \pm 0.1$  °C with fluorocarbon coolant. Sample injection time was 3 s, and detection was by UV (214 nm). Mobility was calculated from the average time to elution of at least two runs:

$$\mu = \frac{lL}{V} \left( \frac{1}{t_m} - \frac{1}{t_s} \right) \quad (1)$$

Here  $l$  is the effective length of the capillary,  $L$  is the total length of the capillary,  $V$  is the applied voltage, and  $t_m$  and  $t_s$  are retention times of the reference marker (mesityl oxide) and the sample, respectively.

**Electrophoretic Light Scattering (ELS).** ELS was carried out at four scattering angles (8.9, 17.6, 26.3, and 35.2°) using a DELSA 440SX apparatus (Coulter Instrument Co.) equipped with a 5 mW He–Ne laser ( $\lambda = 632.8$  nm). The electric field was applied at a constant current of 0.7 mA. The electrophoretic cell had a rectangular cross section connecting the hemispherical cavities in each electrode, and the total sample volume was about 1 mL. The temperature of the thermostated sample chamber was maintained at 25 °C. The measured electrophoretic mobility ( $\mu$ ) was the average value at the stationary layer measured at the above angles. The procedure was checked with the DELSA

mobility standard before the measurement. The mobility values obtained in this work are repeatable within less than 10% error.

## Results and Discussion

**Carboxylation.** The weight ratio of sodium chloroacetate to Ficoll 400 (C/F) was used to control carboxylation. Figure 2 shows that the degree of carboxylation increases upon raising C/F from 5 to 20 but decreases with further increase of C/F to 30. The maximum degree of carboxylation appears after 10 h at C/F = 20.

DLS indicated a broad MWD for carboxylated Ficoll 400. Therefore, CF400(20:1), the sample with the highest charge density, was fractionated into 17 fractions (Table 1) which were characterized by dynamic light scattering and titration. In Table 1, the weight-average molecular weight  $M$  in g/mol is calculated according to

$$M = \left[ \frac{10\pi N_A R_h^3}{3K} \right]^{1/(1+a)} \quad (2)$$

where  $R_h$  is the viscosity radius in cm (here replaced by the apparent hydrodynamic radius measured by DLS in 0.1 M ammonium acetate buffer with pH = 7.0),  $N_A$  is Avogadro's number, and  $K$  and  $a$  are Mark–Houwink coefficients for ficoll ( $K = 0.156$  mL/g,  $a = 0.38$ <sup>12</sup>). It is assumed that any effect of carboxylation on the  $K$  and  $a$  values are suppressed at 0.1 M ionic strength so that  $K$  and  $a$  are unchanged by carboxylation. The charge amount  $Q$  was measured by titration after ion exchange by Dowex resin:

$$Q = \frac{(V - V_b)C}{m/M_w} \quad (3)$$

Here  $V$  and  $V_b$  are the respective volumes in milliliters of NaOH used to titrate carboxylated ficoll and blank sample from pH ca. 3 to the equivalence point (detected as the maximum in  $\Delta\text{pH}/\Delta V$ ),  $C$  is the concentration of NaOH,  $m$  is the amount of carboxylated ficoll sample in milligrams, and  $M_w$  is the weight average molecular weight of carboxylated ficoll sample.

The plot of average charge amounts per molecule determined by titration versus the square of the hydrodynamic radii of each fraction (Figure 3) is linear within reasonable experimental error. This relationship, also observed in separate studies,<sup>15</sup> indicates that carboxylation takes place mainly at the surface so that CF molecules can be considered as surface-charged spheres.

**Mobility from ELS and CE.** The limited amount of CF3.0, CF4.6, and CF7.3 fractions restricted mobility measurements to CE, but CF400 samples were sufficiently abundant to allow us to prepare concentrated samples for ELS measurement. As seen in Figure 4, the CE mobility values for CF400(20:1), CF400(22:1), and CF400(30:1) were higher than those determined by ELS, while the two methods approximately agreed for CF400(10:1).

CE and ELS differ with regard to the magnitude of applied electric field  $E$ , by more than 1 order of magnitude higher for the first. We are aware of no report of a direct comparison between these two methods. Therefore, the CE electric field was changed by varying the applied voltage by a factor of 6. As showed in Figure 5, mobility for several solutes depends on  $E$ , but the slope depends on samples.<sup>16</sup> The mobility of EMPSL7 decreased with increasing  $E$  as it deviates from the standard value of  $-4.33 \pm 0.39 \times 10^{-8}$  m<sup>2</sup>/(V s). On the other hand, CF400(20:1), CF400(22:1), and CF(3.0) have positive slopes with mobility values measured by CE larger than those by ELS

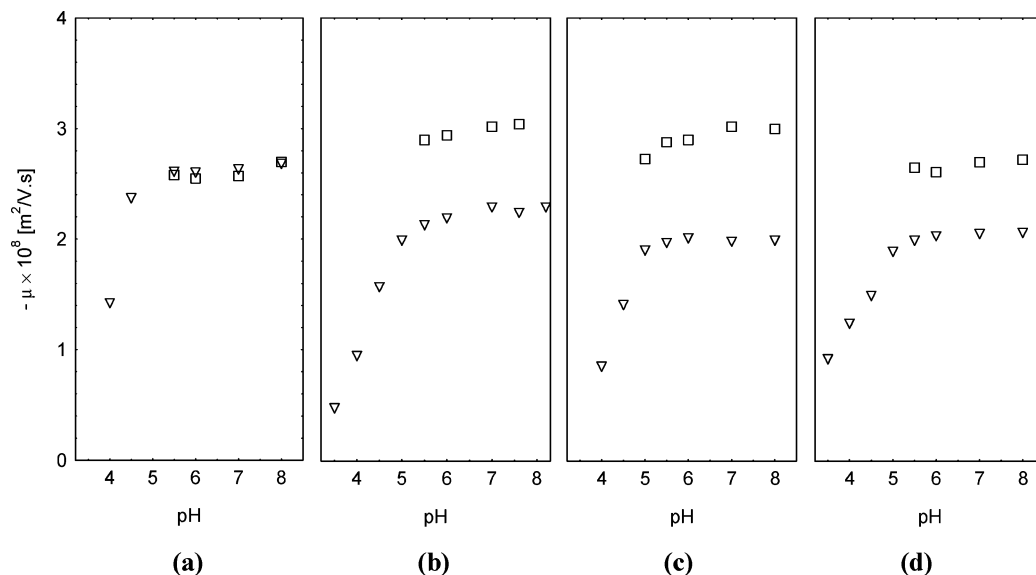


**Figure 4.** Comparison of mobility data determined by CE (□) and by ELS (▽) in 0.1 M phosphate buffer solution: (a) CF400(10:1); (b) CF400(20:1); (c) CF400(22:1); (d) CF400(30:1).

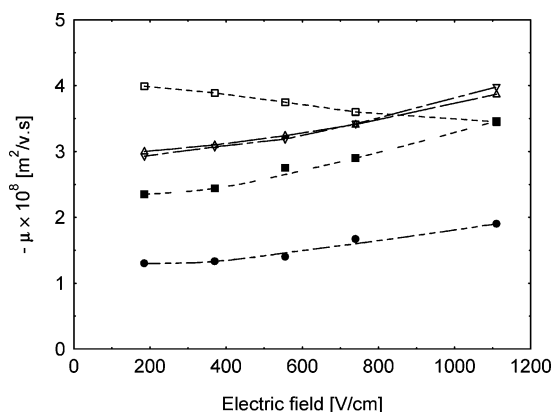


**Figure 5.** Dependence of mobility on electric field of CE in 0.1 M phosphate buffer solution with pH = 7.0: BSA (●); DELSA mobility standard sample EMPSL7 (□); CF(3.0) (■); CF400(22:1) (△); CF400(20:1) (▽).

(see Figure 4b,c). Hoagland et al. observed an increase in  $\mu$  with  $E$  for poly(styrenesulfonate) and attributed it to Joule heating and the resulting drop in viscosity.<sup>17</sup> However, this scenario fails to explain our results for the DELSA standard EMPSL7 and is also inconsistent with strong effects of field on mobility of dendrimers in the absence of Joule heating.<sup>16</sup> The mobilities of BSA and CF(3.0) are almost independent of  $E$  especially when  $E < 370$  V/cm, and the values of  $\mu$  obtained by CE at 370 V/cm agree well with those from ELS (Figure 6). Thus, it should be possible to compare the CE data for CF3.0, CF4.6, and CF7.3 measured at  $E = 185$  V/cm to the ELS data for CF400 samples.

**Mobility Plateaus.** Upon increasing pH, the electrophoretic mobilities of all carboxylated ficolls increase to a plateau at pH around 5.3 (Figure 7). It is necessary to examine the dependence of mobility on dissociation degree  $\alpha$  to explore the origin of the mobility plateau. The degree of ionization  $\alpha$  was deduced from the blank-corrected titration of CF samples with 0.1 N HCl using the procedure for carboxylated amylose of ref 18 (Figure 8) to give the relationship between  $\alpha$  and pH shown in Figure 9. Despite some scatter, the data in Figure 10 show that the mobility plateau appears before full dissociation (i.e. at 70% ionization of all carboxyl groups), which implies that the mobility does not follow the increase of charge amount but

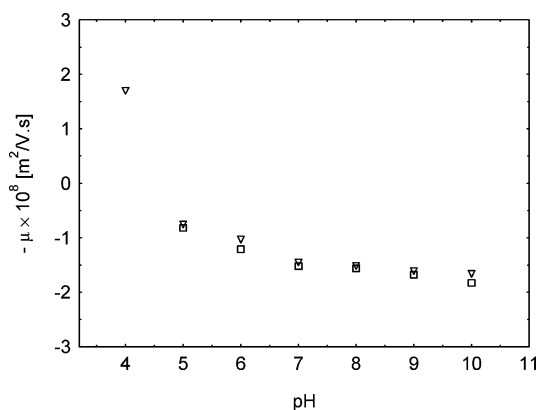


**Figure 6.** Comparison of electrophoretic mobility for BSA in 0.1 M phosphate buffer solution determined by CE (□) at 370 V/cm and by ELS (▽).

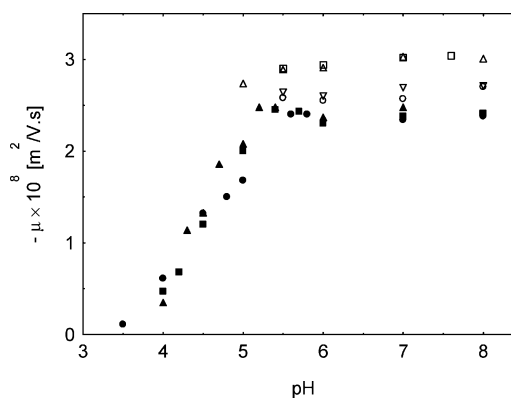


**Figure 7.** Electrophoretic mobility (determined by CE) versus pH. Symbols denote the following: CF400(10:1) (○); CF400(20:1) (□); CF400(22:1) (△); CF400(30:1) (▽); CF3.0 (●); CF4.6 (■); CF7.3 (▲).

becomes nonmonotonic at a critical surface charge density, as predicted by many theories.<sup>1-7</sup>

The surface potential  $\psi_0$  can be determined experimentally according to

$$pK_a - pK_0 = 0.434e\psi_0(\alpha)/kT \quad (4)$$

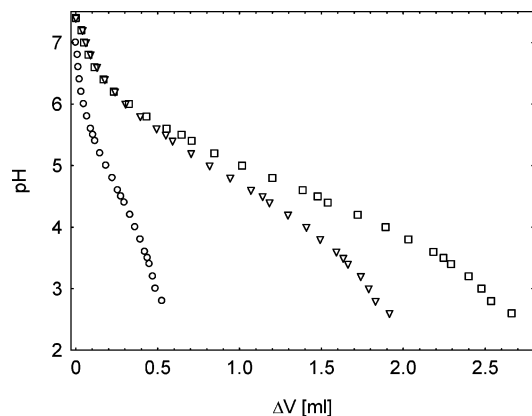


**Figure 8.** pH versus blank-corrected titration volume (0.1 N HCl). Symbols denote the following: 0.0321 g of CF400(10:1) (○); 0.0776 g of CF400(22:1) (□); 0.0486 g of CF400(20:1) (▽).

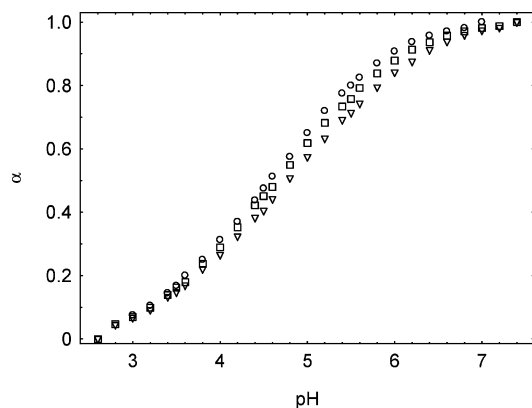


**Figure 9.** pH titration curves ( $\alpha$  versus pH) of CF400 samples. Symbols correspond to the following: CF400(10:1) (○); CF400(22:1) (□); CF400(20:1) (▽).

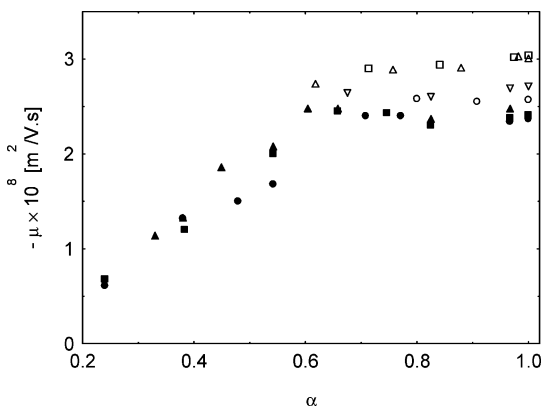


**Figure 10.** Electrophoretic mobility (determined by CE) versus  $\alpha$ . Symbols correspond to the following: CF400(10:1) (○); CF400(20:1) (□); CF400(22:1) (△); CF400(30:1) (▽); CF3.0 (●); CF4.6 (■); CF7.3 (▲).

where  $K_a$  and  $K_0$  are the apparent and the intrinsic dissociation constants respectively,  $e$  is the electron charge,  $k$  is Boltzmann's constant, and  $T$  is absolute temperature.  $K_a$  can be deduced from

$$pK_a = \text{pH} + \log\left(\frac{1-\alpha}{\alpha}\right) \quad (5)$$

where  $pK_0$  is obtained by extrapolating  $pK_a$  to  $\alpha = 0$ . The dependences of  $pK_a$  and  $\psi_0$  on  $\alpha$  for CF400 samples are displayed in Figure 11.

The  $pK_0$  values of CF400(10:1), CF400(20:1), and CF400(22:1) are  $4.0 \pm 0.2$ ,  $4.1 \pm 0.2$ , and  $4.0 \pm 0.2$ , respectively,

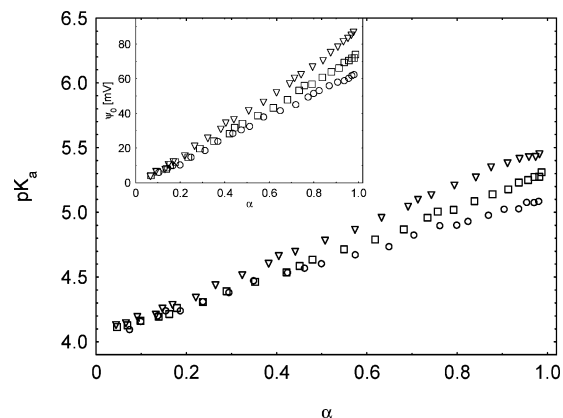


**Figure 11.** Dependence of  $pK_a$  on  $\alpha$ . Symbols denote the following: CF400(10:1) (○); CF400(22:1) (□); CF400(20:1) (▽). Inset: Surface potential versus  $\alpha$ .

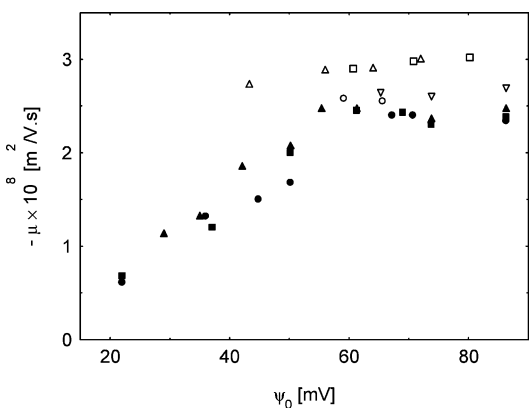


**Figure 12.** Dependence of electrophoretic mobility (determined by CE) on the surface potential. Symbols denote the following: CF400(10:1) (○); CF400(20:1) (□); CF400(22:1) (△); CF400(30:1) (▽); CF(3.0) (●); CF(4.6) (■); CF(7.3) (▲).

which are slightly less than those of dendrimers with carboxyl end groups ( $4.4 \pm 0.13$ ).<sup>19</sup> The excessive crowding of carboxylic acids in the latter might stabilize the acid form via H-bonding, thus leading to a positive  $pK$  shift. The surface potential  $\psi_0$  shows a linear dependence on  $\alpha$  (Figure 11), consistent with the dependence of  $\psi_0$  on  $\sigma$  from the Gouy–Chapman equation in spherical dimensions.<sup>20</sup> Consequently, the mobility plateau is also seen in its dependence on surface potential (Figure 12).

Counterion condensation has been invoked in the context of the nonmonotonic mobility of dendrimers,<sup>11</sup> partly by way of analogy to the observation of a discontinuity in the mobility of polyelectrolytes when the Manning parameter<sup>21</sup> exceeds its critical value.<sup>22–24</sup> In that case, the condensed counterions are accumulated close to the charged rod of the polyelectrolyte and remain present at infinite dilution of the polyelectrolyte system. Zimm and Le Bret<sup>25</sup> have considered the surface geometry in the phenomenon of counterion condensation, concluding that condensation always occurs for the flat plane, sometimes for the cylinder, and never for the sphere. Since counterion accumulation has not been demonstrated at infinite dilution, the term “condensation” will not be applied to charged spheres such as ficolls, and we will be similarly circumspect in using the ambiguous “binding”. Instead, we shall investigate the accumulation of counterions in two experimentally accessible regions of the EDL: close to the surface where their presence reduces the surface potential ( $\psi_0$ ); within the shear plane where their presence reduces the mobility and hence the  $\zeta$  potential. Such populations will be referred to as surface potential-determining ions and mobility-determining ions, respectively.

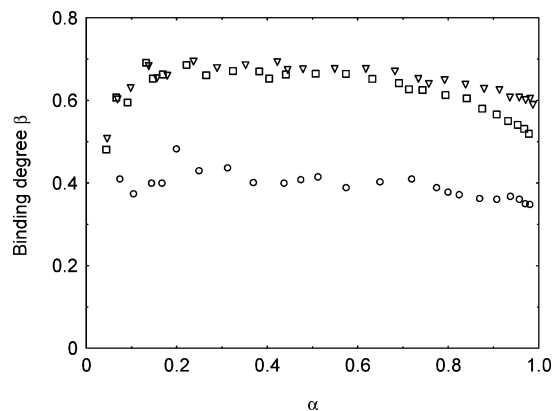


**Figure 13.** Counterion binding degree  $\beta$  versus  $\alpha$ . Symbols denote the following: CF400(10:1) (○); CF400(20:1) (□); CF400(22:1) (△).

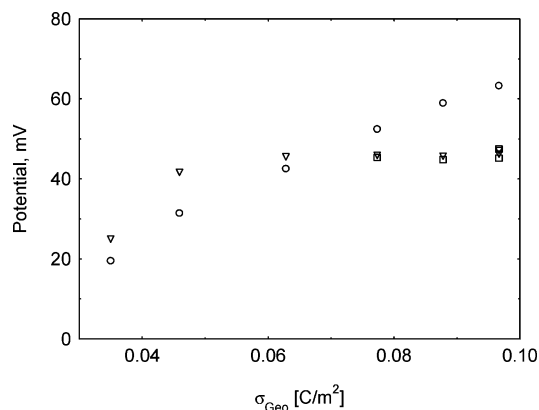


**Figure 14.** Comparison of surface and  $\zeta$  potentials as a function of surface charge density for CF400(10:1). Symbols denote the following: surface potential (○);  $\zeta$  potentials determined by CE (□) and ELS (△).

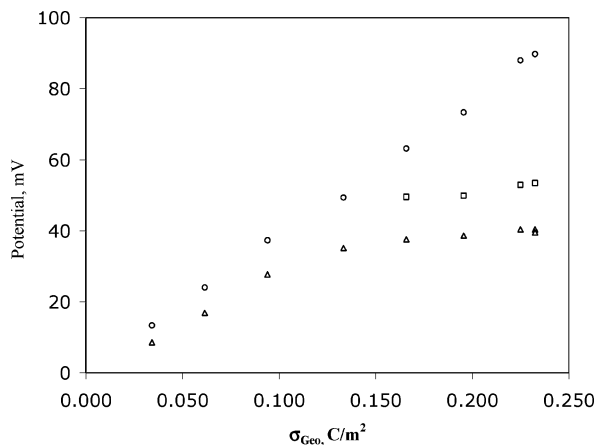


**Figure 15.** Comparison of surface and  $\zeta$  potentials as a function of surface charge density for CF400(20:1). Symbols denote the following: surface potential (○);  $\zeta$  potentials determined by CE (□) and ELS (△).

The remaining counterions beyond the shear plane are considered to be diffuse or free.

For further insight into the origin of mobility plateau, surface potentials from the titration data were used to calculate effective surface charge densities using the numerical solutions to the Poisson–Boltzmann equation as given by Loeb, Overbeek, and Wiersema.<sup>26</sup> Using a  $q_0$  value equal to  $\kappa a$  (9.67), values of the integral function  $I(q_0, y_0)$  were interpolated from the tables to

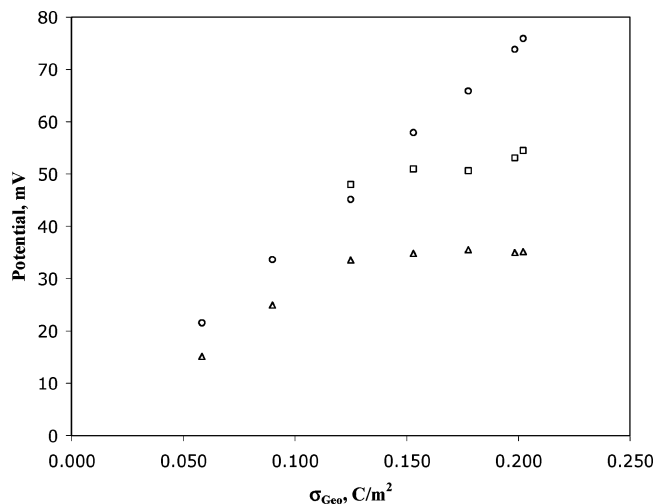


**Figure 16.** Comparison of surface and  $\zeta$  potentials as a function of surface charge density for CF400(22:1). Symbols denote the following: surface potential (○);  $\zeta$  potentials determined by CE (□) and ELS (△).

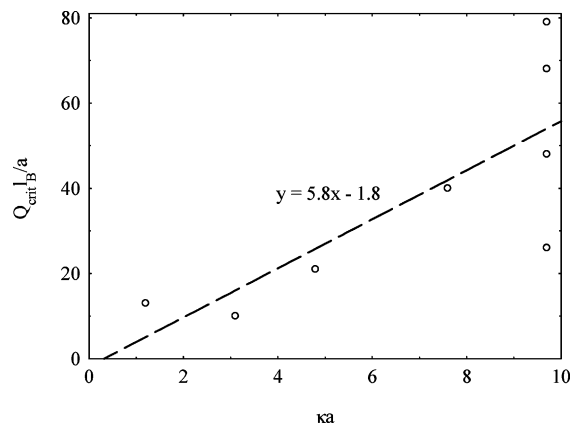


**Figure 17.** Critical values of the geometric surface charge as  $(Q_{\text{crit},B}/a)$  versus  $\kappa a$ . The linear regression curve for the data is also shown.

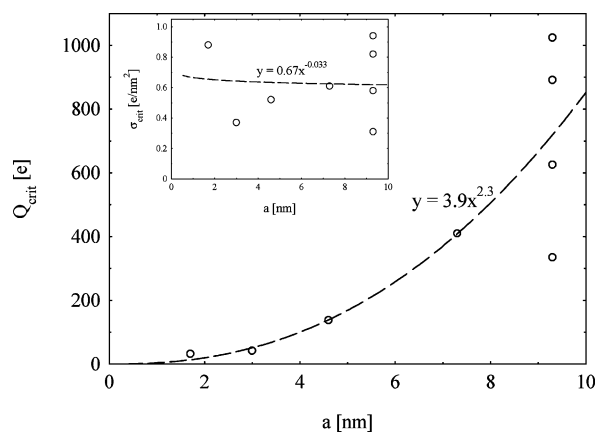


**Figure 18.** Critical geometric charge of colloid as a function of colloid radius. The line shows the power law regression curves for the data. Inset: Critical geometric surface charge density as a function of colloid radius.

determine the effective  $\sigma$  and then the effective charge  $Q_{\text{eff}}$ . The counterion binding degree is given as

$$\beta = 1 - \frac{Q_{\text{eff}}}{Q_{\text{geom}}} \quad (6)$$

where  $Q_{\text{geom}}$  is the geometric surface charge based on the titration end points. Since  $Q_{\text{eff}}$  is obtained from surface

TABLE 2: Critical Conditions for the Appearance of a Mobility Plateau

| sample      | $a$ (nm) | $\kappa a$ | $\alpha_c$ | $\psi_{0c}$ (mV) | $\sigma_c$ (e/nm <sup>2</sup> ) |      | $Q_{cl_B}/a$ (e) |     |
|-------------|----------|------------|------------|------------------|---------------------------------|------|------------------|-----|
|             |          |            |            |                  | geom                            | eff  | geom             | eff |
| G2          | 1.7      | 1.2        | 0.89       | 84               | 0.88                            | 0.62 | 13               | 9.4 |
| G5          | 3.7      | 2.7        | 0.77       | 66               | 4.35                            | 0.33 | 140              | 11  |
| CF(3.0)     | 3.0      | 3.1        | 0.71       | 63               | 0.37                            | 0.44 | 10               | 12  |
| CF(4.6)     | 4.6      | 4.8        | 0.64       | 57               | 0.52                            | 0.36 | 21               | 15  |
| CF(7.3)     | 7.3      | 7.6        | 0.60       | 53               | 0.61                            | 0.31 | 40               | 20  |
| CF400(10:1) | 9.3      | 9.7        | 0.51       | 34               | 0.31                            | 0.18 | 26               | 15  |
| CF400(20:1) | 9.3      | 9.7        | 0.65       | 56               | 0.94                            | 0.33 | 79               | 28  |
| CF400(22:1) | 9.3      | 9.7        | 0.65       | 47               | 0.82                            | 0.27 | 68               | 22  |
| CF400(30:1) | 9.3      | 9.7        | 0.68       | 64               | 0.58                            | 0.39 | 48               | 33  |

potentials, the “bound counterions” here are the surface potential-determining ions. Figure 13 shows that the value of  $\beta$  is fairly constant and increases with degree of carboxylation. The  $\zeta$  potential would then be predicted to increase monotonically with increasing ficoll ionization, and so  $\mu$  should increase monotonically with the surface potential. In order for the mobility plateau to be explained entirely by surface binding of counterions,  $\beta$  would have to increase significantly at  $\alpha$  values above 0.6 or 0.7, unlike the result in Figure 13. Given the mobility plateaus, there must be an accumulation of counterions inside the shear plane (defined here as mobility-determining ions) other than the surface potential-determining ions.

$\zeta$  potentials were calculated from the mobility values determined by both CE and ELS, using Henry’s equation:<sup>20</sup>

$$\mu = \frac{2\epsilon_0\epsilon_r}{3\eta} \zeta [f_1(\kappa a)] \quad (7)$$

Here the function  $f_1(\kappa a)$  is 1.24, the dielectric constant  $\epsilon_r$  is 78.5,  $\epsilon_0$  is  $8.854 \times 10^{-12} \text{ C V}^{-1} \text{ m}^{-1}$ , and the viscosity  $\eta$  is  $0.00101 \text{ N s m}^{-2}$ . Values of  $\zeta$  are plotted together with  $\psi_0$  from potentiometric titration in Figures 14–16. At high degrees of ionization,  $\zeta$  does not follow the monotonic rise in  $\psi_0$  with increasing surface charge density which would be expected from the Poisson–Boltzmann equation for a spherical colloid<sup>20</sup> with a constant shear plane distance  $x$  and a fixed  $\kappa$  value:

$$\zeta = \psi_0 \frac{R e^{-\kappa x}}{R + x} \approx \psi_0 e^{-\kappa x} \quad (8)$$

Here  $R$  is the colloid radius. There are two ways to account for the apparent diminution of  $\zeta$  at high surface potential relative to its expected value: an increase in the distance to the shear plane  $x$  to enclose more counterions in the kinetic unit; an increase in local ionic strength, hence  $\kappa$ , due to accumulation of counterions within the shear plane. On the basis of eq 8 and with an assumption of no accumulation of surface potential-determining ions, the shear plane distance was estimated to be about 0.15 nm for CF400(10:1) and about 0.30 nm for CF400(20:1) and CF400(22:1). The values are reasonable given that the distance should be of the order of a few water molecules;<sup>27</sup> however, these estimated distances are dependent on both Henry’s equation (eq 7) and the model for the electrostatic potential function in the electric double layer.

**Critical Conditions for the Appearance of the Mobility Plateau.** The values of the dissociation degree, surface potential, and surface charge density at the appearance mobility plateaus ( $\alpha_c$ ,  $\psi_{0c}$ , and  $\sigma_c$ , respectively) obtained from Figures 10 and 12 are collected in Table 2 as a function of colloid radius. Both geometric (from titration) and effective (from potentiometry) critical charge values are shown. In Table 2,  $a$  is the colloid radius,  $\kappa$  is the inverse of the Debye length,  $Q_c$  is the critical

surface charge valency, and  $l_B$  is the Bjerrum length (0.714 nm at 25 °C). The titration data from the CF400(20:1) sample were applied to the monodisperse ficoll samples since these had the same degree of carboxylation as the polydisperse sample. The geometric charge of monodisperse ficolls were obtained from the established relationship between radius and total charge (Figure 3) for fractionated ficoll samples having radii  $< 7.5$  nm. Data of carboxyl-terminated dendrimers G2 and G5 in Table 2 came from ref 10.

Without specifically denoting surface potential-determining ions as “condensed”, we can still follow the general approach of Manning, namely that counterions are bound to the macroion if the electrostatic attraction energy between the two is much higher than thermal energy  $kT$ .<sup>21</sup> For a charged sphere, the criterion becomes<sup>11,28,29</sup>

$$\frac{a^2}{l_B Q} \ll \kappa^{-1} \quad \frac{l_B Q}{a} \gg \kappa a \quad (9)$$

Inspection of Table 2 reveals that the criterion in eq 9 is satisfied by having the critical value of  $(Q/l_B)/a$  exceed  $\kappa a$ , typically by a factor of 3–11 when the geometric charge is used for  $Q$ . This ratio decreases when the effective charge,  $Q_{\text{eff}}$ , is used in place of  $Q_{\text{geom}}$ , due to the surface-potential determining ions. The ratio for G5 dendrimer is unusually large when geometric charge is used, but its electrophoretic behavior is consistent with those of carboxylated ficolls of similar radii. The accumulation of mobility-determining ions beyond the critical surface charge thus appears to have a similar basis to the Manning condensation of counterions.

Figure 17 shows that the geometric surface charge required for the plateau in mobility, in the form of  $(Q_{\text{geom}}/l_B)/a$ , is linear with  $\kappa a$  for the colloids, with the exception of the G5 dendrimer. The slope of the regression line suggests a critical ratio of  $(Q_{\text{geom}}/l_B)/a$  to  $\kappa a$  of 5.8, which compares well to the prediction of a critical ratio of 4 by Belloni<sup>28</sup> for counterion accumulation onto spheres. Figure 18 shows that the critical geometric surface charge is nearly a linear function of the colloid radius squared, suggesting a common critical surface density for the appearance of the mobility plateau. Calculated critical surface charge densities fluctuate about 0.6 charges/nm<sup>2</sup> (or about  $0.10 \text{ C}\cdot\text{m}^{-2}$ ), as seen in Table 2 and Figure 18.

The critical surface potentials,  $\psi_{0c}$ , are plotted as a function of particle radius in Figure 19. The required surface potentials are well above that of thermal energy (25.7 mV) for the colloids investigated, supporting the energy criterion in eq 9. A reciprocal relationship is observed for the critical surface potential, further demonstrating that the mobility plateau is not simply due to the surface-potential determining ion population and accumulation of mobility-determining ions is easier for larger colloids than for smaller colloids of the same surface potential.

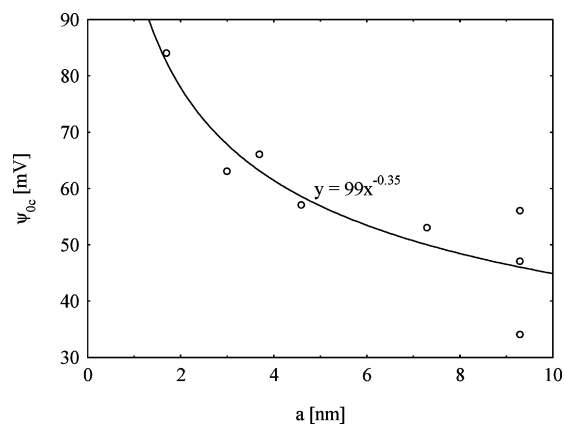


**Figure 19.** Critical surface potential as a function of colloid radius. The solid line represents an exponential fitting of experimental data.

## Conclusion

Nanosized carboxylated ficolls (CF) were synthesized and then characterized by potentiometric titration, capillary electrophoresis (CE), and electrophoretic light scattering (ELS). Behavior consistent with simple electrostatic models indicates that charges are uniformly distributed on their surfaces, making these ideal model systems to investigate the electrophoretic mobility of charged spheres with sizes intermediate between those of dendrimers and latex particles. Mobility plateaus were observed when a critical value was exceeded for the degree of ionization,  $\alpha$ , or the surface potential,  $\psi_0$ . Given similar plateaus for charged dendrimers and charged latex particles, these appear to be general features for charged spheres. The critical conditions were found to correspond to a criterion for strong binding, analogous to Manning counterion condensation on polyelectrolytes. In this case, the accumulation of surface potential-determining ions is revealed by potentiometric titration, which shows a constant degree of binding with increasing colloid charge. Beyond the surface, mobility-determining ions accumulate within the shear plane, and it is the increase in this population when the surface charge exceeds a critical value that explains the mobility plateau. The remaining counterions form the diffuse part of the electric double layer.

Because the accumulation of mobility-determining counterions observed for charged ficolls qualitatively and quantitatively agrees with the counterion condensation analogy for spheres presented by Belloni,<sup>28</sup> further investigation by theoreticians is warranted. Manning's theory of counterion condensation is based upon the principle of balancing the loss of entropy of free counterions (equal to  $k_B T \ln V$ , where  $V$  is the solution volume accessible to counterions) to the gain of electrostatic energy in being condensed. According to Zimm and Le Bret,<sup>25</sup> condensation always occurs for a charged plane, sometimes occurs for the infinite charged cylinder, but never occurs for the isolated charged sphere. For the case of cylindrical geometry, both the counterion entropy and electrostatic energy scale as logarithms, so a balance is achieved at a critical linear charge

density. The electrostatic energy in the spherical geometry scales as charge-to-radius ratio (finite), and so cannot outweigh the loss of entropy of the counterions. But the possibility of counterion condensation to spheres is shown theoretically by Ramanathan<sup>30</sup> to be a limiting condition when the radius exceeds the Debye length, a condition in which the geometry of the sphere approaches that of a plane.

**Acknowledgment.** Support from NSF Grant CHE 0345382 is acknowledged. We thank Prof. A. Dobrynin for insightful suggestions.

## References and Notes

- (1) Lozada-Cassou, M.; Gonzalez-Tovar, E. *J. Colloid Interface Sci.* **2001**, *239*, 285.
- (2) Wiersema, P. H.; Loeb, A. L.; Overbeek, J. Th. G. *J. Colloid Interface Sci.* **1966**, *22*, 78.
- (3) O'Brien, R. W.; White, L. R. *J. Chem. Soc., Faraday Trans. 2* **1978**, *74*, 1607.
- (4) Degreve, L.; Lozada-Cassou, M.; Sanchez, E.; Gonzalez-Tovar, E. *J. Chem. Phys.* **1993**, *98*, 8905.
- (5) Gonzalez-Tovar, E.; Lozada-Cassou, M. *J. Phys. Chem.* **1989**, *93*, 3761.
- (6) Lozada-Cassou, M.; Saavedra-Barrera, R. *J. Chem. Phys.* **1982**, *77*, 5150.
- (7) Henderson, D.; Lozada-Cassou, M.; Blum, L. *J. Chem. Phys.* **1983**, *79*, 3055.
- (8) Martin-Molina, A.; Quesada-Perez, M.; Galisteo-Gonzalez, T.; Hidalgo-Alvarez, R. *J. Phys. Chem. B* **2002**, *106*, 6881.
- (9) Schulz, S. F.; Sticher, H. *Prog. Colloid Polym. Sci.* **1994**, *97*, 85.
- (10) Welch, C. F.; Hoagland, D. A. *Langmuir* **2003**, *19*, 1082.
- (11) Huang, Q. R.; Dubin, P. L.; Moorefield, C. N.; Newkome, G. R. *J. Phys. Chem. B* **2000**, *104*, 898.
- (12) Lavrenko, P. N.; Mikryukova, O. I.; Didenko, S. A. *Polym. Sci. U.S.S.R.* **1986**, *28*, 576.
- (13) Davidson, M. G.; Deen, W. M. *Macromolecules* **1988**, *21*, 3474.
- (14) Zhu, Y.; Potschka, M.; Dubin, P. L.; Cai, C. *Macromol. Chem. Phys.* **2001**, *202*, 61.
- (15) Mark, L. A. Modeling of Glomerular Basement Membrane as a Charged Fiber-Matrix. Ph.D. Thesis, Indiana University, Indianapolis, IN, Sep 2001.
- (16) Seyrek, E.; Dubin, P. L.; Newkome, G. R. *J. Phys. Chem. B* **2004**, *108*, 10168.
- (17) Starkweather, M. E.; Hoagland, D. A.; Muthukumar, M. *Macromolecules* **2000**, *33*, 1245.
- (18) Dubin, P. L.; Brant, D. A. *Macromolecules* **1975**, *8*, 831.
- (19) Zhang, H.; Dubin, P. L.; Kaplan, J.; Moorefield, C. N.; Newkome, G. R. *J. Phys. Chem. B* **1997**, *101*, 3494.
- (20) Hunter, R. J. *Foundations of Colloid Science*; Clarendon Press: New York, 1992; Vol. I.
- (21) Manning, G. S. *J. Chem. Phys.* **1969**, *51*, 924.
- (22) Whitlock, L. R. In *New Directions in Electrophoretic Methods*; Jorgenson, J. W., Phillips, M., Eds.; ACS Symposium Series 335; American Chemical Society: Washington, DC, 1987.
- (23) Gao, J. Y.; Dubin, P. L.; Sato, T.; Morishima, Y. *J. Chromatogr., A* **1997**, *766*, 233.
- (24) Klein, J. W.; Ware, B. R. *J. Chem. Phys.* **1984**, *80*, 1334.
- (25) Zimm, B. H.; Le Bret, M. *J. Biomol. Struct. Dyn.* **1983**, *1*, 461.
- (26) Loeb, A. L.; Overbeek, J. Th. G.; Wiersema, P. H. *The Electric Double Layer Around a Spherical Colloid Particle*; MIT Press: Cambridge, MA, 1961.
- (27) Hiemenz, P. C. *Principles of colloid and surface chemistry*, 2nd ed.; M. Dekker: New York, 1986.
- (28) Belloni, L. *Colloid Surf., A* **1998**, *140*, 227.
- (29) Dobrynin, A. University of Connecticut, Storrs, CT, personal communication, 2002.
- (30) Ramanathan, G. V. *J. Chem. Phys.* **1988**, *88*, 3887.